ORGANOMETALLICS

pubs.acs.org/Organometallics

Article

Understanding the Influence of Lewis Acids on CO_2 Hydrogenation: The Critical Effect Is on Formate Rotation

Ljiljana Pavlovic* and Kathrin H. Hopmann*

Cite This: *Organometallics* 2023, 42, 3025−3035

Read Online

ACCESS | Metrics & More | Article Recommendations | Supporting Information

ABSTRACT: Lewis acids (LAs) have been shown to accelerate hydrogenation of CO_2, but the underlying mechanistic details remain to be elucidated. We have employed computational methods to investigate how LAs affect CO_2 hydrogenation with a range of known metal-hydrides (L_nIr-H, L_nRu-H, L_nMn-H, L_nCo-H). Our results show that LAs can alter the nature of the hydride−CO_2 bond formation step, but do not lower its barrier. Instead, the accelerating effect of LAs is on the subsequent step, the rearrangement of the metal-formate σ-intermediate. These insights are essential for understanding the effect of LA additives on metal-mediated hydrogenations of CO_2.

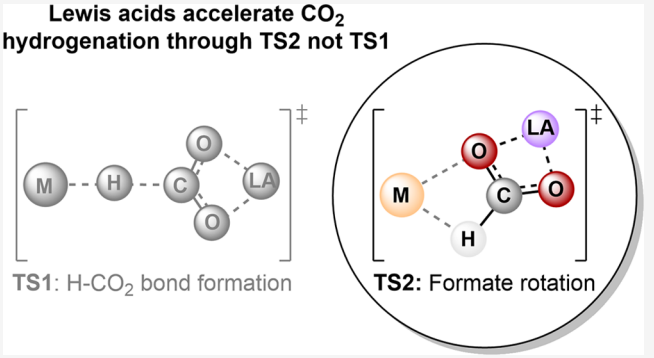

INTRODUCTION

Formic acid is a valuable feedstock employed in agriculture as well as pharmaceutical and textile industries.[1−5] It also has potential as a hydrogen storage medium.[6−10] There is increasing focus on developing synthetic strategies for the production of formate from sustainable resources such as CO_2, a widely accessible and cheap carbon source.[11−30] However, utilization of CO_2 in hydrogenations or other chemical transformations remains challenging, due to the inertness and thermal stability of CO_2. Strategies for CO_2 activation are therefore of great importance, with one promising approach involving use of Lewis acid (LA) additives.[31−41]

Hazari and co-workers have shown that alkali-based LAs significantly accelerate CO_2 hydrogenation and formate dehydrogenation, involving Fe, Mn, Ni, Ir, and Ru complexes.[31−34,39−41] In particular lithium-based LAs appear to have beneficial effects. Addition of LiOTf improved CO_2 hydrogenation in several studies involving first-row transition metals, including iron, manganese, and cobalt compounds.[31,32,34,35,39] Klankermayer and co-workers reported that turnover numbers for hydrogenation of CO_2 with an *in situ* generated nickel-catalyst could be enhanced 3-fold by addition of $LiBF_4$ or LiCl.[36] Interestingly, the use of $B(C_6F_5)_3$ or $Zn(OTf)_2$ provided marginal effects. On the other hand, Romero et al. reported that $B(C_6F_5)_3$ is crucial for CAAC-Cu-catalyzed hydrogenation of CO_2.[37] Also for precious metal systems such as $[Ru(tpy)(bpy)H]PF_6$, Hazari and co-workers reported rate enhancements for CO_2 insertion into the metal-hydride bond with LiOTf or $LiPF_6$ additives.[40] Sodium- and potassium-based LAs provided less effects. The authors hypothesized that smaller, acidic cations provide better stabilization of the negative charge developing on CO_2 during H−CO_2 bond formation.[40] Kinetic studies demonstrated that alkali-based LAs also enhance the rate of CO_2 insertion into an Ir−hydride system, by up to 100-fold.[33] Best effects were obtained with bulky and more dissociative alkali LAs such as $LiNTf_2$, $LiBPh_4$·3DME, and $NaBArF_4$.[33]

Despite the large number of experimental studies reporting that LA additives are beneficial for metal-mediated CO_2 hydrogenation (and formate dehydrogenation),[14,18,19,31−35,37,40,42−45] the underlying mechanistic details are not fully understood. For insertion of CO_2 into metal−R bonds (R = hydride or alkyl/aryl), generally two mechanisms can be considered (Scheme 1A): *i*) An *inner sphere path*, involving an interaction between CO_2 and the metal at the transition state for H−CO_2 bond formation (TS_{inn}).[11,46−49] Note that a precoordination of CO_2 is not required.[50] *ii*) An *outer sphere path*, involving a nucleophilic attack of a ligand onto CO_2 in the absence of a metal−CO_2 interaction (TS1).[11,46,49,51−63] Subsequently, the resulting η^1-σ-intermediate rearranges (TS2)[64,65] to allow for formation of a κ^1-O-(or κ^2-O,O-)carboxylate species. *It is important to note that although TS_{inn} and TS2 both are cyclic, they are entirely different transition states, whose optimized geometries will show distinct features. For CO_2 hydrogenation, a H···CO_2 interaction of ∼1.5−1.7 Å is*

Received: August 1, 2023
Published: October 11, 2023

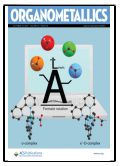

Scheme 1. (A) Mechanisms for CO_2 Insertion into Metal-Hydrides, and (B) Earlier Proposed Interaction between LAs and CO_2 during *Outer Sphere* Hydrogenation[11,31]

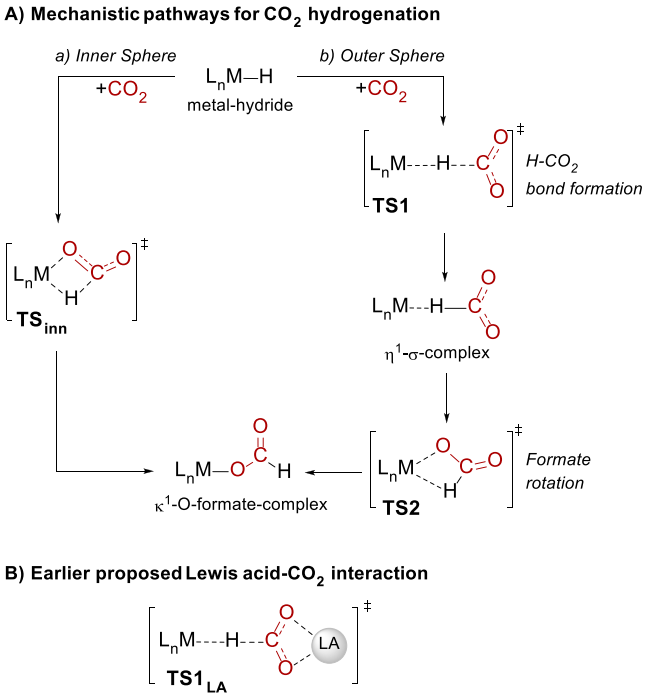

typically observed for TS_{inn},[46,47,66,67] *but less than 1.3 Å for TS2*.[38,56−58,68]

It has been speculated that Lewis acids accelerate CO_2 hydrogenation by stabilizing the emerging negative charge on the oxygen atoms of CO_2 during the H−CO_2 bond formation step (Scheme 1B).[31,33,40] Such stabilizing effects were proposed to be most pronounced in an *outer sphere* mechanism, which could explain why some CO_2 hydrogenation reactions are not accelerated by LAs, as they may proceed through an *inner sphere* pathway.[33] However, for many experimental systems, the mechanistic details are not known, such that it is not possible at this point to conclude if there is a widespread correlation between the effect of LA additives and the mechanistic pathway (*inner* or *outer sphere*). Furthermore, there are very few mechanistic studies on the effect of LAs on CO_2 hydrogenation. Bertini et al. used DFT-methods to study the reduction of CO_2 with a PNP-Mn(I)-catalyst in the presence of DBU and LiOTf,[38] showing that the σ-intermediate formed after H−CO_2 bond formation is several kcal/mol more stable if coordinated to $[Li(THF)_2]^+$. However, the effect of LAs on the involved transition states was not explored. The CO_2 insertion into a rhenium-hydride in the presence of BF_3 (as a computational model of $B(C_6F_5)_3$) was examined by Berke and co-workers using DFT-methods,[69] but only the first step (H−CO_2 bond formation) was analyzed, while the reorganization of the σ-complex was not evaluated. Similarly, Esteruelas and co-workers studied the TS for formate dehydrogenation with an Os−Ge bimetallic complex, reporting an interaction between CO_2 and the acidic Ge center at the H−CO_2 bond cleavage step, but the effect of Ge on the TS for formate rotation was not investigated.[70]

If LAs accelerate CO_2 hydrogenation, it may be expected that the critical effect is on a rate-limiting step of the reaction. Interestingly, several computational studies have shown that for *outer sphere* CO_2 hydrogenation, rearrangement of the metal-formate σ-complex to a κ^1-O-species (TS2, Scheme 1A) appears to have a higher barrier than the H−CO_2 bond formation (TS1).[38,56−58,68] On the basis of this, we hypothesize that the rate-accelerating effect of Lewis acids on CO_2 hydrogenation primarily may be on formate rotation (TS2), not on H−CO_2 bond formation (TS1).

To assess our hypothesis, we chose a representative set of four experimentally known CO_2 hydrogenation reactions involving metal-hydrides based on Ir, Ru, Mn, and Co (Figure 1). Our

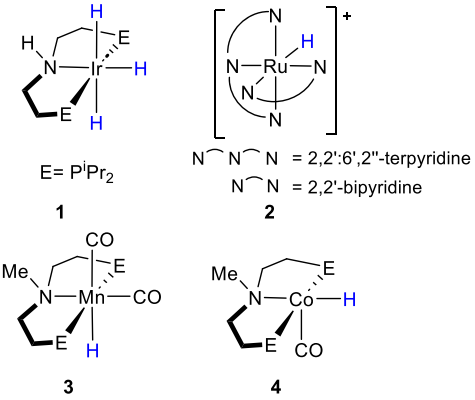

Figure 1. Schematic representation of the complexes studied computationally here (from refs 32−34,40).

computational models predict that all four systems undergo *outer sphere* CO_2 hydrogenation, which in the absence of LAs display larger barriers for formate rotation (TS2) than for H−CO_2 bond formation (TS1). Interestingly, although addition of LAs to the computational model changes the geometries of the H−CO_2 bond formation (TS1), the barriers of this step are not reduced. However, in line with our hypothesis, the transition states for formate rotation (TS2) show significantly lower barriers in the presence of lithium-based LAs. Our results provide a mechanistic understanding of the LA effect on CO_2 hydrogenation, which so far has been lacking.

COMPUTATIONAL DETAILS

The software package Gaussian 16 Rev. C.01[71] was employed for all calculations. The DFT functional PBE0[72,73] was used along with the Grimme empirical dispersion correction (D3BJ)[74] and the conductor-like polarizable continuum model CPCM[75,76] (solvent: THF or CH_3CN, as indicated in the text). For comparison, an additional computational protocol was applied (B3LYP-D3,[74,77] SI, Tables S3−S6). For geometry optimizations, basis set BS1 was employed, which includes the split-valence double-ζ Ahlrichs basis set def2-SVP[78] on all atoms (except on F where def2-SVPD[78] was used) and the LANL2TZ[79] basis set and pseudopotential on Ru, Mn, Co, and Ir. For single point electronic energy calculations, the basis set BS2 was employed, which consists of def2-TZVP on all atoms (except on F where def2-TZVPD was used) and LANL2TZ(f) on Ru, Mn, Co, and Ir. The computed free energies ($\Delta G^\circ_{1\ atm}$, BS1) were converted to the 1M standard state energies employing a standard state (SS)[80] conversion term. At 298 K, the SS correction is −1.89 kcal/mol going from 2 to 1 mol. All calculations were performed at 298 K. A counterpoise correction was computed at the BS2 level for the CO_2 insertion step (SI, Table S1). The standard state Gibbs free energies ($\Delta G^\circ_{1M,298K}$) reported in the main text correspond to

https://doi.org/10.1021/acs.organomet.3c00342
Organometallics 2023, 42, 3025−3035

$$\Delta G^{\circ}_{1M,298K} = \Delta G_{1atm,298K,BS1} - \Delta E_{1atm,BS1} + \Delta E_{1atm,BS2} + CP_{BS2} + SS_{298K}$$

Kinetic isotope effects (KIE) were computed as a ratio of rate constants of the reaction with hydrogen over the reaction with deuterium (for more details see SI, Table S2). IRC calculations were performed on Ir- and Ru-systems in the absence and presence of LiOTf (SI, Figures S6−S11, S27−S30, S34−S37, S50−S53).

All chemical systems were computed without any truncations or symmetry constraints. The conformational space was evaluated carefully through optimization of multiple configurations, with the energetically preferred structures reported here (relevant higher lying geometries are given in the SI). For reaction pathways, both *inner* and *outer sphere* mechanisms were attempted for all systems. However, during unconstrained geometry optimizations, the *inner sphere* TS would in several instances rearrange into an *outer sphere* arrangement.

RESULTS AND DISCUSSION

Ir-Mediated Hydrogenation of CO_2. Hazari and coworkers have shown that the stoichiometric insertion of CO_2 into the trihydride complex [Ir(^{iPr}PN^{H}P)H$_3$] (**1**) is accelerated up to 100-fold by cationic LAs.[33] In presence of LiOTf, the experimentally determined barrier for CO_2 insertion is reduced by 2.9 kcal/mol compared to the LA-free reaction (Scheme 2).[33]

Scheme 2. Previously Reported Effect of LiOTf on the Experimentally Measured Barrier for Stoichiometric CO_2 Hydrogenation with 1[33]

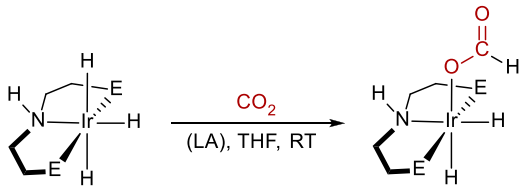

1 (E=P^{i}Pr$_2$)

No LA: $\Delta G^{\ddagger}_{exp}$ = 14.3 kcal/mol
LA = LiOTf: $\Delta G^{\ddagger}_{exp}$ = 11.4 kcal/mol

We have investigated the **1**-mediated hydrogenation of CO_2 computationally in the absence and presence of LAs (SI, Figures S1−S5). The LA-free reaction preferably proceeds through an *outer sphere* H−CO_2 bond formation (**TS1$_{Ir}$**, Figure 2), in line with previous computational results on **1**.[51] **TS1$_{Ir}$** has a barrier of 8.5 kcal/mol and displays a stabilizing hydrogen bond between CO_2 and the N−H backbone (2.00 Å). An alternative cyclic TS1 geometry, involving interaction of CO_2 with iridium, is 7.2 kcal/mol higher in energy, making it unlikely (SI, Figure S3). IRC calculations confirm that after H−CO_2 bond formation, a σ-complex is formed (SI, Figures S6−S11).

The σ-intermediate (SI, Figure S4) has been proposed to dissociate into formate and a cationic iridium-complex[51] (in line with earlier work by Ahlquist[56]); however, we find such a step nonfeasible, with a computed cost of 24.6 kcal/mol for dissociation of formate from iridium (SI, Figure S72A). Instead, we propose that the σ-intermediate rearranges to a κ^1-O-formate complex (SI, Figure S5) through a formate rotation via **TS2$_{Ir}$** (Figure 2), as suggested for related *outer sphere* CO_2 insertions.[38,58,68] IRC calculations confirm that TS2 indeed connects the σ-intermediate and the κ^1-O-formate complex (SI, Figures S6−S11). The computed barrier for **TS2$_{Ir}$** of 16.7 kcal/mol is feasible at room temperature and is in line with the experimentally reported overall barrier of 14.3 kcal/mol for this reaction (we note that absolute barriers can vary with different DFT functionals, however, computed trends are similar, see SI, Tables S3−S6).[81] *Our results show that for **1**-mediated CO_2 hydrogenation, the formate rotation is rate-limiting, implying that this step needs to be considered when additive effects are evaluated.*

We proceeded to compute the effect of adding LiOTf to the computational model, assuming that it will not dissociate to a large extent (in contrast to, e.g., LiPF$_6$ or LiBArF$_4$, *vide infra*).[33,82,83] Initially, LiOTf forms an adduct with **1**, displaying weak interactions with one of the hydrides (1.77 Å, Figure S12). Additionally, one oxygen of triflate forms a strong interaction with the NH backbone (2.00 Å). Interestingly, this complex is able to weakly bind CO_2 to iridium (Ir−CO_2 2.15 Å, Figure S13), with a cost of 6.9 kcal/mol. The subsequent H−CO_2 bond formation preferably takes place through a *cyclic* transition state **TS1$_{IrLiOTf(cyc)}$** (barrier 11.3 kcal/mol), where CO_2 interacts with the metal (2.19 Å, Figure 2), making iridium seven-coordinated and indicating Ir(V) character. At the TS, lithium interacts with both oxygen atoms of CO_2 (2.00 Å, 2.01 Å), which is significantly bent (122.6°). We note that an alternative linear H−CO_2 bond formation TS1 also was optimized in the presence of LiOTf (**TS1$_{IrLiOTf-1}$**, SI, Figure S14A), but is 5.1 kcal/mol higher in energy. *Our findings indicate that LiOTf changes the chemical nature of TS1 from linear to cyclic for **1** but does not lower the barrier of this step.*

Interestingly, the subsequent formate rotation displays a barrier reduction from 16.7 to 11.1 kcal/mol in the presence of LiOTf (Figure 2). The geometric features of **TS2$_{IrLiOTf}$** appear little affected, with small changes in bond lengths compared to the LA-free case, indicating that the barrier reduction largely is caused by charge stabilization. This effect is so pronounced that TS1 becomes rate-limiting for **1**-mediated hydrogenation of CO_2 in the presence of LiOTf. It can be noted that the overall computed barrier reduction of 5.4 kcal/mol (from 16.7 to 11.3 kcal/mol) is larger than the experimentally predicted reduction of 2.9 kcal/mol (Scheme 2). We assume that the stabilizing effect of the solvent (THF) in the LA-free reaction is underestimated in our model, leading to a small overestimation of the computed LA effect. *Nonetheless, our results clearly predict that the beneficial effect of LiOTf on **1**-mediated CO_2 hydrogenation is on the formate rotation step (TS2), not the H−CO_2 bond formation (TS1).*

It has been reported that [Li(solvent)$_n$]$^+$ complexes can be formed from lithium salts containing weakly coordinating anions such as NTf$_2^-$, PF$_6^-$, BF$_4^-$, or BArF$_4^-$.[40,82] In the known crystal structures of solvated Li-complexes, the number of coordinated solvent molecules varies from 1 to 4.[45,84−87] Here, we have compared the results for nondissociated LiOTf (Figure 2) as well as LiNTf$_2$ to the cationic solvent complexes [Li(THF)$_2$]$^+$ and [Li(THF)$_3$]$^+$ (SI, Figure S17−S26), to evaluate if the LA effect on the barriers is dependent on the coordination environment around Li. As Table 1 shows, all tested LA species significantly lower the barrier of TS2 compared to the LA-free case, implying that this trend is independent of the coordination environment. However, the absolute barriers differ, with the solvated complexes showing lower barriers than the neutral LAs; this effect can be ascribed to better charge stabilization. In this context we emphasize that the computed barriers are relative to a reference state of the Ir-hydride···LA adduct, and some

https://doi.org/10.1021/acs.organomet.3c00342
Organometallics 2023, 42, 3025−3035

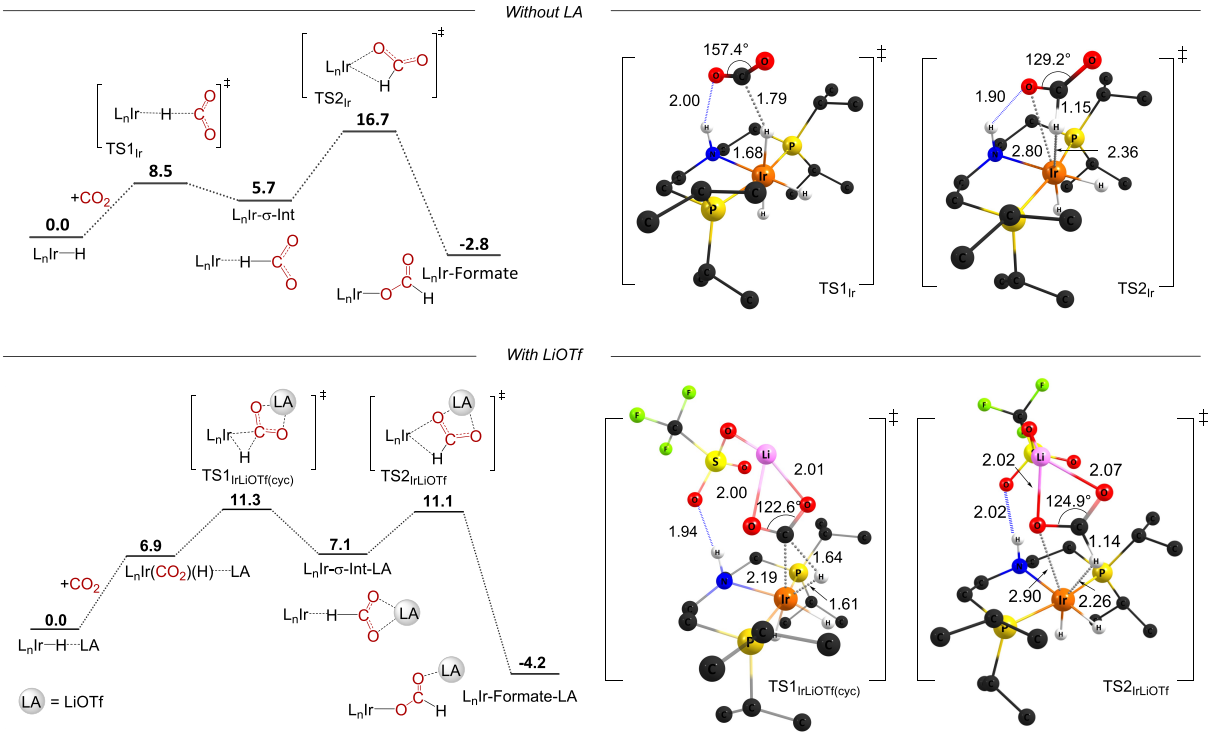

Figure 2. Energies and optimized TS geometries for CO_2 insertion into **1** in absence (top) and presence (bottom) of LiOTf ($\Delta G_{1M,298K}$, PBE0-D3BJ, CPCM[THF], distances in angstrom, H atoms omitted except for relevant interactions).

Table 1. Computed Barriers (kcal/mol) for 1-Mediated Hydrogenation of CO_2 in the Presence of Li-Complexes

LA in model	$\Delta G^{\ddagger}$ TS1	$\Delta G^{\ddagger}$ TS2	$\Delta\Delta G^{\ddagger}_{(TS2\text{-}TS1)}$
LiOTf	11.3	11.1	−0.2
$LiNTf_2$	10.7	10.7	0.0
$[Li(THF)_2]^+$	9.0	9.4	+0.4
$[Li(THF)_3]^+$	6.7	5.4	−1.3

uncertainty in the *absolute* numbers can be expected. However, the barrier differences between TS1 and TS2 are independent of the chosen reference state. We find that LiOTf, $LiNTf_2$, and $[Li(THF)_2]^+$ give close to identical barriers for $TS1_{Ir}$ and $TS2_{Ir}$ (within 0.0 to 0.4 kcal/mol), whereas the model with $[Li(THF)_3]^+$ displays a rate-limiting TS1, which has a 1.3 kcal/mol higher barrier than TS2. The coordination environment around Li may thus affect which step becomes a rate-limiting step in cases where the two steps have comparable energies in the presence of LAs.

Ru-Mediated Hydrogenation of CO_2. In order to establish if the results observed for **1** indicate a general trend for the effect of LAs on CO_2 hydrogenation, we proceeded to analyze the stoichiometric insertion of CO_2 into $[Ru(tpy)(bpy)H]^+$ (**2**).[40] Experimentally, also this reaction is accelerated by addition of LAs, with LiOTf and $LiNTf_2$ showing similar results (Scheme 3).

On the basis of previous computational studies,[43] the **2**-mediated hydrogenation of CO_2 has been proposed to occur through a single step, reminiscent of *inner sphere* CO_2 insertion (Scheme 1). However, our computational analysis indicates that the stoichiometric CO_2 insertion into **2** occurs in two steps, through an *outer sphere* pathway (Figure 3, SI, Figures S31−S33). The computed barrier for the first step, H−CO_2 bond formation ($\mathbf{TS1_{Ru}}$), is 11.4 kcal/mol (Figure 3, top). The optimized geometry displays a close to linear configuration, with

Scheme 3. Previously Reported Effect of LAs on the Barriers and Rates of Stoichiometric [2]PF_6-Mediated CO_2 Hydrogenation[40,88]

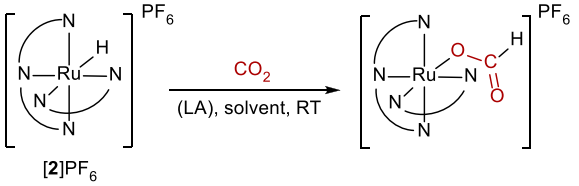

solvent = ^{i}PrOH

No LA: $\Delta G^{\ddagger}_{exp}$ = 18.9 ± 0.3 kcal/mol
LA = $LiNTf_2$: $\Delta G^{\ddagger}_{exp}$ = 15.0 ± 0.3 kcal/mol
LA = $B(OiPr)_3$: $\Delta G^{\ddagger}_{exp}$ = 16.5 ± 0.3 kcal/mol

solvent = CH_3CN

LA = LiOTf: k_{LA} = 3.0 ± 0.3 M^{-2} s^{-1}
LA = $LiNTf_2$: k_{LA} = 3.1 ± 0.3 M^{-2} s^{-1}
LA = $KBPh_4$: k_{LA} = 2.1(2) × 10^{-1} M^{-2} s^{-1}
LA = $B(OiPr)_3$: k_{LA} = 7.9(8) × 10^{-2} M^{-2} s^{-1}

CO_2 being weakly stabilized through a C−H/O interaction with the bipyridine ring (2.32 Å). IRC calculations confirm that $\mathbf{TS1_{Ru}}$ is connected with a Ru-σ-complex (SI, Figures S34−S37). Rearrangement of the σ-intermediate ($\mathbf{TS2_{Ru}}$) has a barrier of 20.8 kcal/mol, significantly higher than TS1, in line with the results for **1**. Again, we evaluated if dissociation of formate from the σ-complex may be an alternative pathway to forming the κ^1-O-formate; however, the dissociated complex has an energy of 24.7 kcal/mol, which is higher than $\mathbf{TS2_{Ru}}$ (SI, Figure S72B). The overall computed barrier for CO_2 insertion into **2** of 20.8 kcal/mol in CH_3CN is 1.9 kcal/mol above the experimentally determined value for [**2**]PF_6 in ^{i}PrOH solvent (18.9 ± 0.3, Scheme 3).[40] We assume that protic ^{i}PrOH

https://doi.org/10.1021/acs.organomet.3c00342
Organometallics 2023, 42, 3025−3035

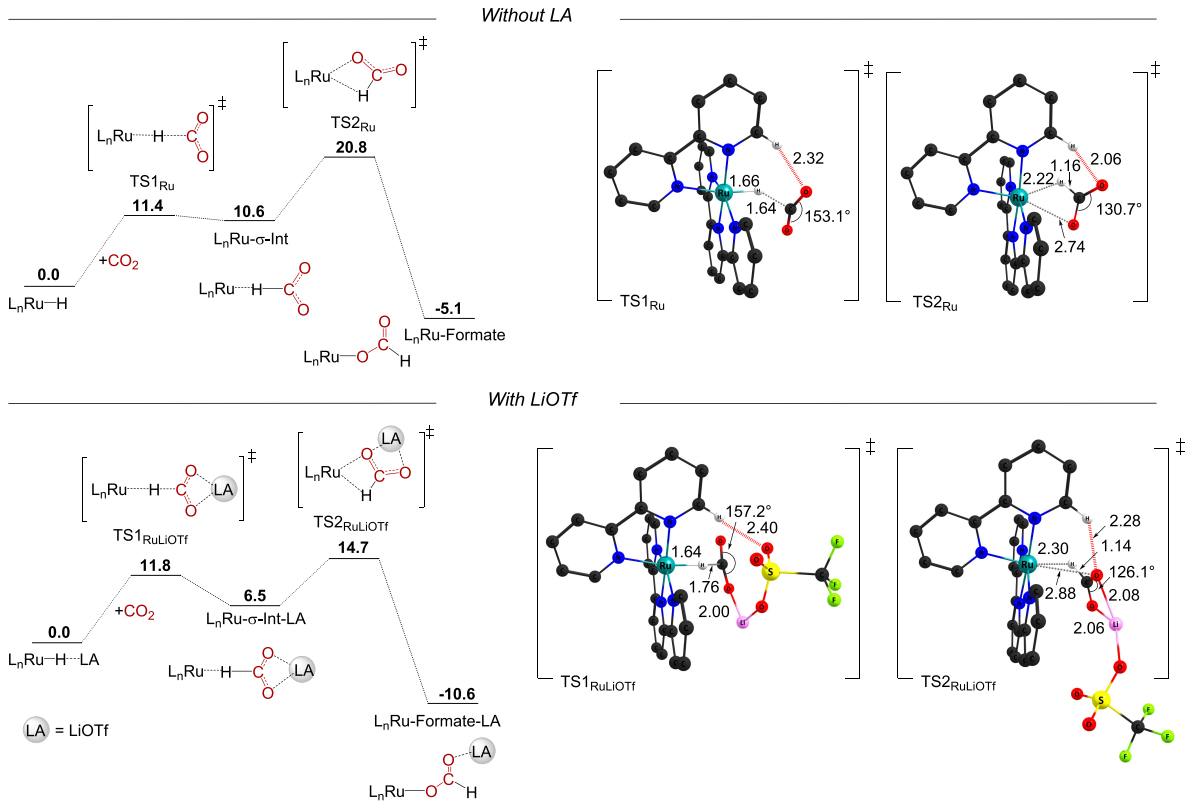

Figure 3. Energies and optimized TS geometries for CO_2 insertion into **2** in absence (top) and presence (bottom) of LiOTf ($\Delta G_{1M,298K}$, PBE0-D3BJ, CPCM[CH_3CN], distances in angstrom, H atoms omitted except for relevant interactions).

provides better charge stabilization during the reaction than CH_3CN, which is supported by a faster rate in ^{i}PrOH than in CH_3CN in experiments.[40]

We proceeded to compute the effect of adding LiOTf to the computational model of **2**. The energetic reference is a **2**−LiOTf adduct, which displays several noncovalent interactions between LiOTf and the Ru complex (SI, Figure S38). For outer sphere CO_2 insertion into **2**, the optimized $\mathbf{TS1_{RuLiOTf}}$ displays a linear geometry, making it different from the iridium case (*vide supra*).[89] At the TS, Li interacts with one oxygen of CO_2 (2.00 Å) whereas the second oxygen is far away (4.10 Å). The computed barrier for $\mathbf{TS1_{RuLiOTf}}$ is 11.8 kcal/mol, in line with the barrier in absence of LA ($\mathbf{TS1_{Ru}}$, 11.4 kcal/mol, Figure 3). *This indicates that LiOTf has no beneficial effect on the H−CO_2 bond formation step of* **2**.

Interestingly, the barrier for the Ru-mediated formate rotation ($\mathbf{TS2_{RuLiOTf}}$) decreases by 6.1 kcal/mol in the presence of LiOTf. *Our results indicate that the accelerating effect of LiOTf is on TS2, also for* **2**. At $\mathbf{TS2_{RuLiOTf}}$, Li forms two interactions with the oxygen atoms of the CO_2 (2.06 Å, 2.08 Å, Figure 3). The resulting κ^1-O-formate-complex (SI, Figure S40) is 5.5 kcal/mol more stable than in the absence of LiOTf. The overall computed barrier of 14.7 kcal/mol for insertion of CO_2 into **2** in the presence of LiOTf (in CH_3CN) resembles the experimentally determined free energy barrier of 15.0 kcal/mol in the presence of the related LA $LiNTf_2$ (in ^{i}PrOH, Scheme 3).[40]

In order to evaluate if the results for **2** are critically dependent on the coordination environment and dissociation state of lithium, we compared models with solvated $[Li(CH_3CN)_2]^+$ or $[Li(CH_3CN)_3]^+$ complexes (SI, Figures S41−S46), as well as with one (Figure 3) or two LiOTf molecules (Figure 4). The LiOTf-dimer (Figure 4), which may be viewed as a model of a

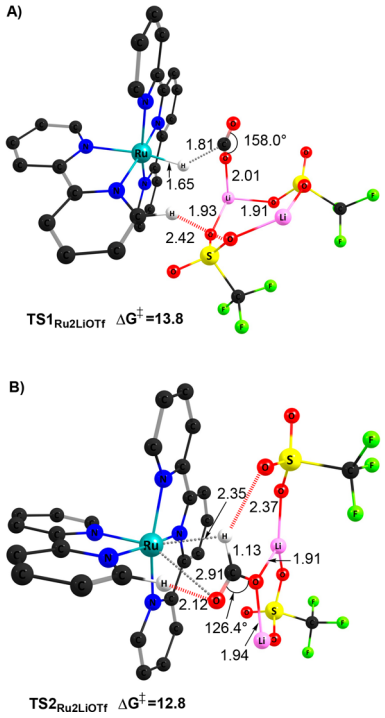

Figure 4. Optimized TS geometries for CO_2 insertion into **2** in the presence of two LiOTfs ($\Delta G_{1M,298K}$, PBE0-D3BJ, CPCM [CH3CN], distances in angstrom, H omitted except for relevant interactions). At TS1, CO_2 interacts with one Li, the other Li moves away during geometry optimizations.

Li-aggregate, displays bridging OTf molecules, in line with known X-ray structures.[85] The results (Table 2) confirm the

https://doi.org/10.1021/acs.organomet.3c00342
Organometallics 2023, 42, 3025−3035

Table 2. Computed Barriers (kcal/mol) for 2-Mediated Hydrogenation of CO_2 in the Presence of Li-Complexes

LA in model	$\Delta G^{\ddagger}$ TS1	$\Delta G^{\ddagger}$ TS2	$\Delta\Delta G^{\ddagger}_{(TS2\text{-}TS1)}$
LiOTf	11.8	14.7	+2.9
$[Li(CH_3CN)_2]^+$	11.9	16.0	+4.1
$[Li(CH_3CN)_3]^+$	15.2	12.8	−2.4
2 × LiOTf	13.8	12.8	−1.0

same trend for all models, with Li significantly lowering the barrier of TS2, but not TS1. In fact, in the presence of $[Li(CH_3CN)_3]^+$ or the LiOTf-dimer, the barrier of TS2 becomes lower than that of TS1 (Table 2). The latter result is worth noting, as LAs typically are used in large excess in experiments, making it plausible that multiple Li-complexes are present at the TS.

Our results have important implications for rationalizing experimental results: for example, measurement of kinetic isotope effects (KIEs) on [**2**]PF_6-mediated CO_2 hydrogenation show an *inverted* KIE in the absence of LAs (0.86 ± 0.09) and no KIE in the presence of 50 equiv of $LiNTf_2$ (1.0 ± 0.1),[40] indicating a change in mechanism or rate-limiting step upon addition of LAs. We have computed the KIEs for the involved TSs and find an *inverted* KIE for TS2 and a *normal* KIE for TS1 (SI, Table S2), in line with recent results for a Re-system.[90] *On the basis of this, we propose that a change in experimental KIE from inverted to normal in the presence of LAs indicates a change in rate-limiting step from formate rotation (TS2) to H−CO_2 bond formation (TS1).*

To validate our computational model further against experiment, we computed the alternative LAs $KBPh_4$ and $B(OiPr)_3$ (Figures 5, S48−S49), which experimentally showed slower reaction rates than LiOTf (Scheme 3). At $\mathbf{TS1}_{\mathbf{RuKBPh4}}$, potassium interacts with only one oxygen of CO_2 (2.78 Å), whereas at $\mathbf{TS2}_{\mathbf{RuKBPh4}}$, it interacts with both oxygens of CO_2 (2.77 and 2.78 Å, Figure 5A). The computed $\mathbf{TS2}_{\mathbf{RuKBPh4}}$ barrier is 2.6 kcal/mol higher than for LiOTf, in line with a smaller rate enhancement observed for $KBPh_4$ (Scheme 3). For $B(OiPr)_3$, the bulky iPr groups only allow for weak interactions between boron and CO_2 at both $\mathbf{TS1}_{\mathbf{RuB(OiPr)3}}$ and $\mathbf{TS2}_{\mathbf{RuB(OiPr)3}}$ (3.64 and 3.48 Å, Figure 5B). The barrier for $\mathbf{TS2}_{\mathbf{RuKBPh4}}$ is 7.2 kcal/mol larger than for LiOTf, in line with the experimental trend, but larger than what would be expected from the difference in rate constants (Scheme 3). The overall results indicate that the strength of the cation−O_{CO2} interaction decreases in the order Li > K ≫ B, in line with previous conclusions that Li^+ is better suited to stabilize CO_2 than K^+.[40]

Mn-Catalyzed Hydrogenation of CO_2. In order to evaluate if the computed LA effect also applies to base metals, we analyzed the catalytic Mn(I)-mediated hydrogenation of CO_2 with H_2.[34] With [MeN{$CH_2CH_2(PiPr_2)$}$_2$]-MnH(CO)$_2$ (**3**), under identical reaction conditions, an increase in TON from 50 to 7950 was reported upon addition of LiOTf (Scheme 4).[34]

Our analysis indicates a two-step *outer sphere* CO_2 insertion pathway for **3** (Figure 6, SI, Figures S54−S57). In the absence of LAs, the computed barriers are 14.5 and 19.5 kcal/mol respectively, for H−CO_2 bond formation ($\mathbf{TS1}_{\mathbf{Mn}}$) and formate rotation ($\mathbf{TS2}_{\mathbf{Mn}}$). At both TSs, several C−H/O interactions between CO_2 and the ligand provide some charge stabilization (2.27 Å, 2.52 Å for $\mathbf{TS1}_{\mathbf{Mn}}$, 2.08−2.51 Å for $\mathbf{TS2}_{\mathbf{Mn}}$).

Addition of LiOTf to the computational model results in a Mn(I)-H···LiOTf adduct, where Li coordinates to a CO group

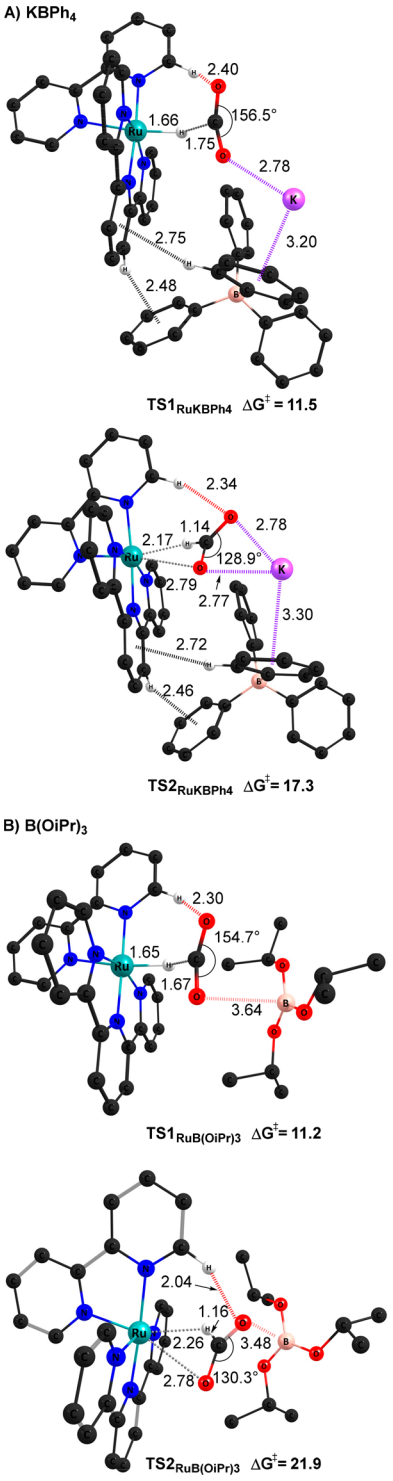

Figure 5. Optimized TS geometries for CO_2 insertion into **2** in the presence of (A) $KBPh_4$ or (B) $B(OiPr)_3$ ($\Delta G_{1M,298K}$, PBE0-D3BJ, CPCM[CH_3CN], distances in angstrom, H atoms omitted except for relevant interactions).

trans to the hydride (Li···O: 1.91 Å, SI, Figure S58). CO_2 insertion into the adduct has a barrier of 16.6 kcal/mol. Interestingly, at $\mathbf{TS1}_{\mathbf{Mn\text{-}LiOTf\text{-}CO}}$, LiOTf prefers to coordinate to CO (1.95 Å) over coordinating to CO_2 (alternative conformations are several kcal/mol higher in energy, Figures S59−S60).

https://doi.org/10.1021/acs.organomet.3c00342
Organometallics 2023, 42, 3025−3035

Scheme 4. (A) Previously Reported Effect of LAs on the Catalytic 3-Mediated CO_2 Hydrogenation, and (B) the Proposed Catalytic Cycle[34]

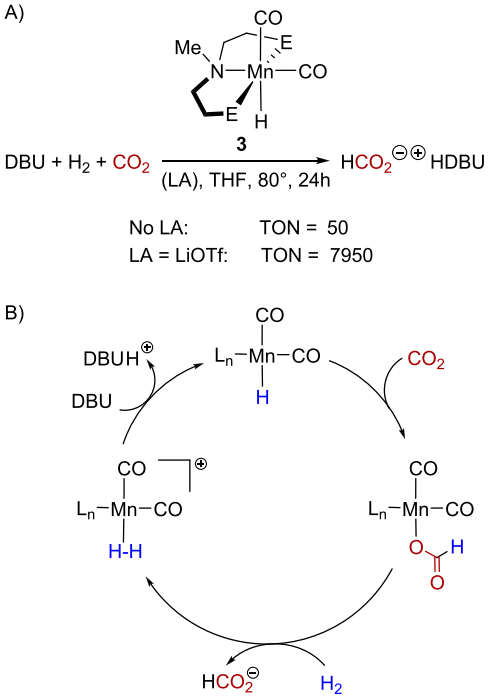

Several C−H/O interactions between CO_2 and the ligand provide charge stabilization. The subsequent formate rotation has a computed barrier of 11.3 kcal/mol (Figure 6), implying a barrier decrease of 8.2 kcal/mol in the presence of LiOTf. At $\mathbf{TS2}_{\mathbf{Mn\text{-}LiOTf\text{-}CO2}}$, Li interacts with both oxygens of CO_2 (2.03 Å, 2.09 Å, another conformation is higher in energy, SI, Figure S62). *Our results indicate that also for* **3**, *LAs have a critical effect on TS2, reducing its barrier below that of TS1.* However, this may *not* imply that TS1 becomes rate-limiting, as the subsequent catalyst regeneration may have a higher barrier, in line with results for other catalytic systems.[35,38,46,47,54,91,92] We computed the catalyst regeneration for **3** (SI, Figure S54), and our results indicate that H_2 association is overall rate-limiting (however, note that the model involves a charge-separation step making evaluation of relative energies challenging, see discussion in SI). Nonetheless, in line with our results for **1** and **2**, we conclude that for **3**, TS2 is more affected by LAs than TS1.

Co-Catalyzed Hydrogenation of CO_2. Finally, we evaluated a Co-analogue of **3**, which can be formed from [^{iPr}PNP-CoH(CO)$_2$]Cl (pre-**4**) with H_2 and DBU.[32] Under catalytic conditions, the active species is proposed to be either **4** or **4b** (Scheme 5). Addition of LiOTf to the reaction increased the TON for pre-**4** from 460 to 10 000, indicating a remarkable accelerating effect.[32]

We attempted to model CO_2 hydrogenation with both **4** and **4b**; however, the latter was unreactive in our computations and did not insert CO_2. For **4**, a CO_2 insertion barrier of 17.3 kcal/mol was obtained ($\mathbf{TS1}_{\mathbf{Co}}$, Figure 7). The barrier for rearrangement of the formed σ-intermediate is high, 32.3 kcal/mol (SI, Figure S64−S66); however, this is in agreement with experiments, where low conversions are reported.[32] Upon addition of LiOTf to the model, the adduct Co(I)-H-LiOTf is formed, where Li interacts with the oxygen of CO (1.93 Å, SI, Figure S67). During H−CO_2 bond formation ($\mathbf{TS1}_{\mathbf{CoLiOTf}}$), lithium interacts with both CO (2.04 Å) and CO_2 (1.97 Å). Several noncovalent C−H/O interactions are seen between the isopropyl groups of the ligand and CO_2 as well triflate

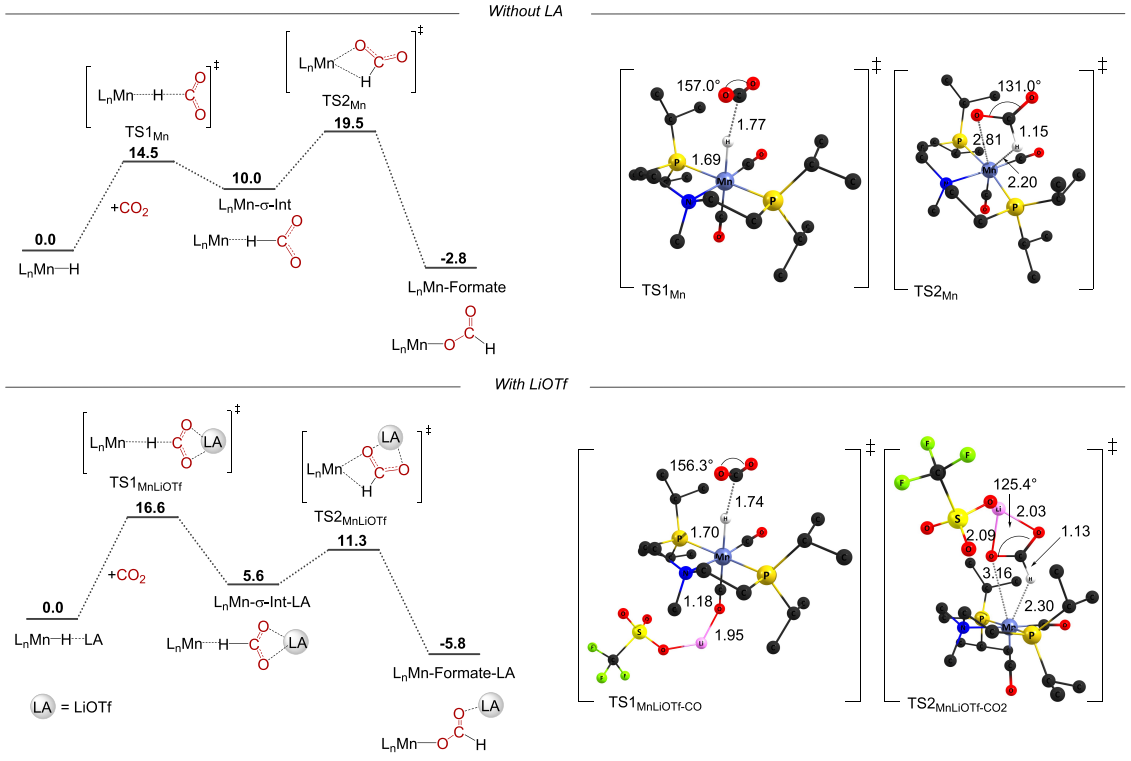

Figure 6. Energies and optimized TS geometries for CO_2 insertion into **3** in absence (top) and presence (bottom) of LiOTf ($\Delta G_{1M,298K}$, PBE0-D3BJ, CPCM[THF], distances in angstrom, H atoms omitted except for relevant interactions).

https://doi.org/10.1021/acs.organomet.3c00342
Organometallics 2023, 42, 3025−3035

Scheme 5. (A) Previously Reported Effect of LiOTf on the Catalytic 4-Mediated CO_2 Hydrogenation and (B) the Proposed Catalytic Cycle[32]

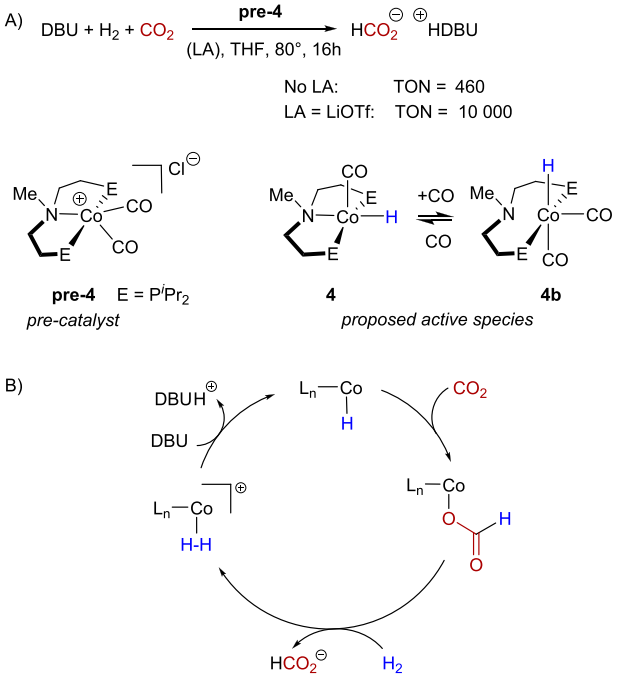

(alternative TS1 geometries are higher in energy, SI, Figure S68). After formation of the σ-intermediate (SI, Figure S69), rotation of formate occurs with a barrier of 23.1 kcal/mol ($\mathbf{TS2}_{\mathbf{CoLiOTf}}$, Figure 7). At the TS, Li interacts with only one oxygen of CO_2 (1.84 Å) which is in contrast to the Ir-, Ru-, and Mn-systems, where Li interacts with both oxygens of CO_2 (such a TS configuration is higher in energy for **4**, SI, Figure S70). *Our results for 4 show that in the presence of LiOTf, the barrier for formate rotation decrease by 9.2 kcal/mol, again establishing that TS2 is more affected by LAs than TS1.*

CONCLUSIONS

In conclusion, we have studied how Lewis acids (LAs) alter the mechanistic details of CO_2 insertion into metal-hydrides. Our computational analyses of four experimentally known complexes based on Ir, Ru, Mn, and Co show that in absence of LAs, all four systems follow an *outer sphere* mechanism, where H−CO_2 bond formation (TS1) has a lower barrier than the rearrangement of the σ-intermediate to a κ^1-O-formate (TS2). Upon addition of LAs to the computational models, the chemical nature of the H−CO_2 bond formation step may alter, as observed for Ir−H, which changes from a linear to a cyclic TS geometry in the presence of LiOTf. However, the TS1 barriers appear little affected by LAs, with most computational models predicting a small barrier increase for TS1 in the presence of lithium-based LAs. *Instead, the beneficial effect of LAs appears to be on the rearrangement of the metal-formate σ-intermediate (TS2), with a computed barrier decrease in the range of 5.6 to 9.2 kcal/mol with LiOTf.* Depending on the nature of the added LA and its degree of solvation, the barrier of TS2 may become lower than TS1, which can explain experimentally observed changes in the KIE upon addition of LAs.[40] Our insights are essential to understand the effect of Lewis acids on CO_2 hydrogenations, allowing for a more rational approach toward the design of new CO_2-converting reactions.

ASSOCIATED CONTENT

Supporting Information

The Supporting Information is available free of charge at https://pubs.acs.org/doi/10.1021/acs.organomet.3c00342.

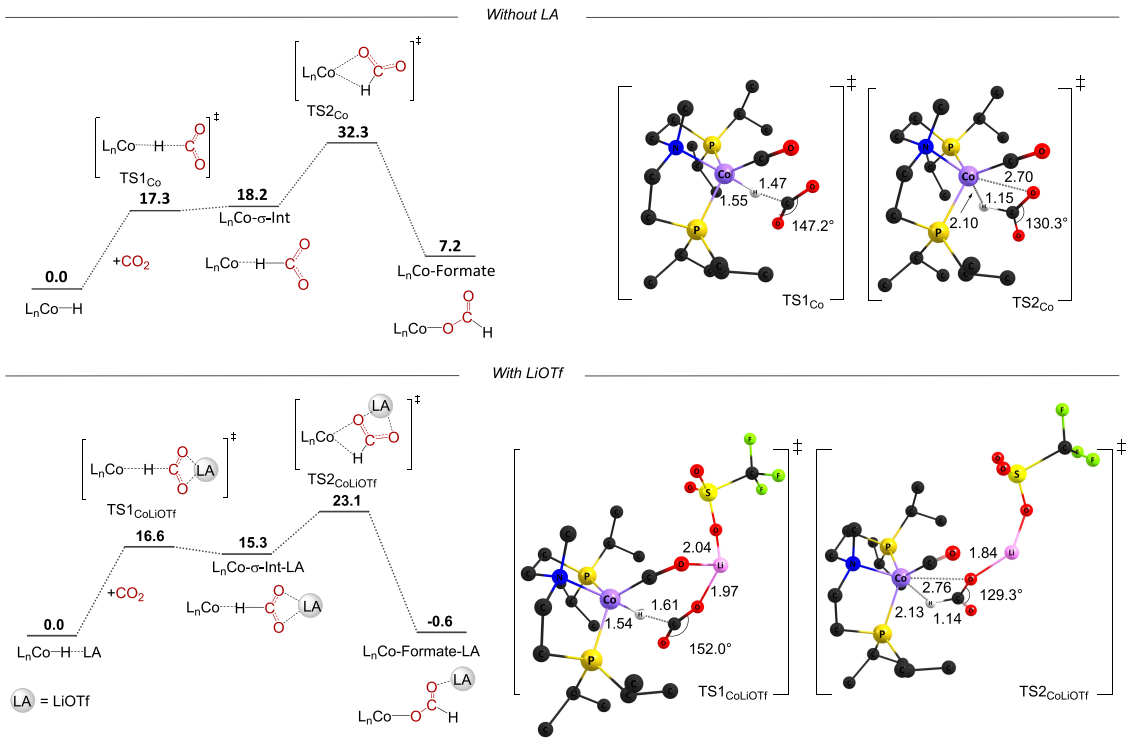

Figure 7. Energies and optimized TS geometries for CO_2 insertion into **4** in absence (top) and presence (bottom) of LiOTf ($\Delta G_{1M,298K}$, PBE0-D3BJ, CPCM[THF], distances in angstrom, H atoms omitted except for relevant interactions).

https://doi.org/10.1021/acs.organomet.3c00342
Organometallics 2023, 42, 3025−3035

Additional computational results, as described in the main text (PDF)

Optimized coordinates, which can be conveniently visualized with the Mercury program from the Cambridge Crystallographic Data Centre (XYZ)

AUTHOR INFORMATION

Corresponding Authors

Ljiljana Pavlovic − *Department of Chemistry, UiT - The Arctic University of Norway, 9037 Tromsø, Norway;* orcid.org/0000-0002-0906-6298; Email: ljiljana.pavlovic@uit.no

Kathrin H. Hopmann − *Department of Chemistry, UiT - The Arctic University of Norway, 9037 Tromsø, Norway;* orcid.org/0000-0003-2798-716X; Email: kathrin.hopmann@uit.no

Complete contact information is available at: https://pubs.acs.org/10.1021/acs.organomet.3c00342

Notes

The authors declare no competing financial interest.

ACKNOWLEDGMENTS

We gratefully acknowledge support from the Research Council of Norway (No. 300769), Sigma2 (Nos. nn9330k and nn4654k), and NordForsk (No. 85378).

REFERENCES

(1) Ricke, S. C.; Dittoe, D. K.; Richardson, K. E. Formic Acid as an Antimicrobial for Poultry Production: A Review. *Front. Vet. Sci.* **2020**, *7*, No. 563.

(2) Aksu, T.; Baytok, E.; Karslı, M. A.; Muruz, H. Effects of formic acid, molasses and inoculant additives on corn silage composition, organic matter digestibility and microbial protein synthesis in sheep. *Small Rumin. Res.* **2006**, *61*, 29−33.

(3) Ferdous, T.; Jahan, M. S.; Quaiyyum, M. A.; Uddin, M. N. Formic acid pulping of crops residues available in Bangladesh. *Biomass Convers. Biorefin.* **2020**, *10*, 289−297.

(4) Supronowicz, W.; Ignatyev, I. A.; Lolli, G.; Wolf, A.; Zhao, L.; Mleczko, L. Formic acid: a future bridge between the power and chemical industries. *Green Chem.* **2015**, *17*, 2904−2911.

(5) Wilson, R. F.; Wilkins, R. J. Formic acid as a silage additive: Effects of formic acid on fermentation in laboratory silos. *J. Agric. Sci.* **1973**, *81*, 117−124.

(6) Singh, A. K.; Singh, S.; Kumar, A. Hydrogen energy future with formic acid: a renewable chemical hydrogen storage system. *Catal. Sci. Technol.* **2016**, *6*, 12−40.

(7) Joó, F. Breakthroughs in Hydrogen Storage-Formic Acid as a Sustainable Storage Material for Hydrogen. *Chem. Sus. Chem.* **2008**, *1*, 805−808.

(8) Preuster, P.; Albert, J. Biogenic Formic Acid as a Green Hydrogen Carrier. *Energy Technol.* **2018**, *6*, 501−509.

(9) Boddien, A.; Gärtner, F.; Federsel, C.; Sponholz, P.; Mellmann, D.; Jackstell, R.; Junge, H.; Beller, M. CO_2-"Neutral" Hydrogen Storage Based on Bicarbonates and Formates. *Angew. Chem., Int. Ed.* **2011**, *50*, 6411−6414.

(10) Sordakis, K.; Tang, C.; Vogt, L. K.; Junge, H.; Dyson, P. J.; Beller, M.; Laurenczy, G. Homogeneous Catalysis for Sustainable Hydrogen Storage in Formic Acid and Alcohols. *Chem. Rev.* **2018**, *118*, 372−433.

(11) Hazari, N.; Heimann, J. E. Carbon Dioxide Insertion into Group 9 and 10 Metal-Element σ Bonds. *Inorg. Chem.* **2017**, *56*, 13655−13678.

(12) Tanaka, R.; Yamashita, M.; Nozaki, K. Catalytic Hydrogenation of Carbon Dioxide Using Ir(III)-Pincer Complexes. *J. Am. Chem. Soc.* **2009**, *131*, 14168−14169.

(13) Maji, B.; Kumar, A.; Bhattacherya, A.; Bera, J. K.; Choudhury, J. Cyclic Amide-Anchored NHC-Based Cp*Ir Catalysts for Bidirectional Hydrogenation−Dehydrogenation with CO_2/HCO_2H Couple. *Organometallics* **2022**, *41*, 3589−3599.

(14) Chang, J.; Mao, J.-X.; Ding, M.; Zhang, J.; Chen, X. Evaluating the Catalytic Activities of PNCNP Pincer Group 10 Metal Hydride Complexes: Pd-Catalyzed Reduction of CO_2 to the Formic Acid Level with NH_3·BH_3 and $NaBH_4$ under Ambient Conditions. *Inorg. Chem.* **2023**, *62*, 4971−4979.

(15) Singh, T.; Jalwal, S.; Chakraborty, S. Homogeneous First-row Transition-metal-catalyzed Carbon Dioxide Hydrogenation to Formic Acid/Formate, and Methanol. *Asian J. Org. Chem.* **2022**, *11*, No. e202200330.

(16) Álvarez, A.; Bansode, A.; Urakawa, A.; Bavykina, A. V.; Wezendonk, T. A.; Makkee, M.; Gascon, J.; Kapteijn, F. Challenges in the Greener Production of Formates/Formic Acid, Methanol, and DME by Heterogeneously Catalyzed CO_2 Hydrogenation Processes. *Chem. Rev.* **2017**, *117*, 9804−9838.

(17) Ra, E. C.; Kim, K. Y.; Kim, E. H.; Lee, H.; An, K.; Lee, J. S. Recycling Carbon Dioxide through Catalytic Hydrogenation: Recent Key Developments and Perspectives. *ACS Catal.* **2020**, *10*, 11318−11345.

(18) Kanega, R.; Ertem, M. Z.; Onishi, N.; Szalda, D. J.; Fujita, E.; Himeda, Y. CO_2 Hydrogenation and Formic Acid Dehydrogenation Using Ir Catalysts with Amide-Based Ligands. *Organometallics* **2020**, *39*, 1519−1531.

(19) Vollmer, M. V.; Ye, J.; Linehan, J. C.; Graziano, B. J.; Preston, A.; Wiedner, E. S.; Lu, C. C. Cobalt-Group 13 Complexes Catalyze CO_2 Hydrogenation via a Co(-I)/Co(I) Redox Cycle. *ACS Catal.* **2020**, *10*, 2459−2470.

(20) Takaoka, S.; Eizawa, A.; Kusumoto, S.; Nakajima, K.; Nishibayashi, Y.; Nozaki, K. Hydrogenation of Carbon Dioxide with Organic Base by PCIIP-Ir Catalysts. *Organometallics* **2018**, *37*, 3001−3009.

(21) Kar, S.; Goeppert, A.; Prakash, G. K. S. Integrated CO_2 Capture and Conversion to Formate and Methanol: Connecting Two Threads. *Acc. Chem. Res.* **2019**, *52*, 2892−2903.

(22) Aresta, M.; Dibenedetto, A.; Angelini, A. Catalysis for the Valorization of Exhaust Carbon: from CO_2 to Chemicals, Materials, and Fuels. Technological Use of CO_2. *Chem. Rev.* **2014**, *114*, 1709−1742.

(23) Zall, C. M.; Linehan, J. C.; Appel, A. M. A Molecular Copper Catalyst for Hydrogenation of CO_2 to Formate. *ACS Catal.* **2015**, *5*, 5301−5305.

(24) Sen, R.; Goeppert, A.; Surya Prakash, G. K. Homogeneous Hydrogenation of CO_2 and CO to Methanol: The Renaissance of Low-Temperature Catalysis in the Context of the Methanol Economy. *Angew. Chem., Int. Ed.* **2022**, *61*, No. e202207278.

(25) Cokoja, M.; Bruckmeier, C.; Rieger, B.; Herrmann, W. A.; Kühn, F. E. Transformation of Carbon Dioxide with Homogeneous Transition-Metal Catalysts: A Molecular Solution to a Global Challenge? *Angew. Chem., Int. Ed.* **2011**, *50*, 8510−8537.

(26) Creutz, C.; Chou, M. H. Rapid Transfer of Hydride Ion from a Ruthenium Complex to C1 Species in Water. *J. Am. Chem. Soc.* **2007**, *129*, 10108−10109.

(27) Huang, J.; Chen, J.; Gao, H.; Chen, L. Kinetic Aspects for the Reduction of CO_2 and CS_2 with Mixed-Ligand Ruthenium(II) Hydride Complexes Containing Phosphine and Bipyridine. *Inorg. Chem.* **2014**, *53*, 9570−9580.

(28) Wei, D.; Sang, R.; Moazezbarabadi, A.; Junge, H.; Beller, M. Homogeneous Carbon Capture and Catalytic Hydrogenation: Toward a Chemical Hydrogen Battery System. *JACS Au* **2022**, *2*, 1020−1031.

(29) Artz, J.; Müller, T. E.; Thenert, K.; Kleinekorte, J.; Meys, R.; Sternberg, A.; Bardow, A.; Leitner, W. Sustainable Conversion of Carbon Dioxide: An Integrated Review of Catalysis and Life Cycle Assessment. *Chem. Rev.* **2018**, *118*, 434−504.

(30) Kumar, A.; Daw, P.; Milstein, D. Homogeneous Catalysis for Sustainable Energy: Hydrogen and Methanol Economies, Fuels from Biomass, and Related Topics. *Chem. Rev.* **2022**, *122*, 385−441.

(31) Zhang, Y.; MacIntosh, A. D.; Wong, J. L.; Bielinski, E. A.; Williard, P. G.; Mercado, B. Q.; Hazari, N.; Bernskoetter, W. H. Iron catalyzed CO_2 hydrogenation to formate enhanced by Lewis acid co-catalysts. *Chem. Sci.* **2015**, *6*, 4291−4299.
(32) Spentzos, A. Z.; Barnes, C. L.; Bernskoetter, W. H. Effective Pincer Cobalt Precatalysts for Lewis Acid Assisted CO_2 Hydrogenation. *Inorg. Chem.* **2016**, *55*, 8225−8233.
(33) Heimann, J. E.; Bernskoetter, W. H.; Hazari, N.; Mayer; James, M. Acceleration of CO_2 insertion into metal hydrides: ligand, Lewis acid, and solvent effects on reaction kinetics. *Chem. Sci.* **2018**, *9*, 6629−6638.
(34) Hert, C. M.; Curley, J. B.; Kelley, S. P.; Hazari, N.; Bernskoetter, W. H. Comparative CO_2 Hydrogenation Catalysis with MACHO-type Manganese Complexes. *Organometallics* **2022**, *41*, 3332−3340.
(35) Kostera, S.; Weber, S.; Peruzzini, M.; Veiros, L. F.; Kirchner, K.; Gonsalvi, L. Carbon Dioxide Hydrogenation to Formate Catalyzed by a Bench-Stable, Non-Pincer-Type Mn(I) Alkylcarbonyl Complex. *Organometallics* **2021**, *40*, 1213−1220.
(36) Schieweck, B. G.; Westhues, N. F.; Klankermayer, J. A highly active non-precious transition metal catalyst for the hydrogenation of carbon dioxide to formates. *Chem. Sci.* **2019**, *10*, 6519−6523.
(37) Romero, E. A.; Zhao, T.; Nakano, R.; Hu, X.; Wu, Y.; Jazzar, R.; Bertrand, G. Tandem copper hydride-Lewis pair catalysed reduction of carbon dioxide into formate with dihydrogen. *Nat. Catal.* **2018**, *1*, 743−747.
(38) Bertini, F.; Glatz, M.; Gorgas, N.; Stöger, B.; Peruzzini, M.; Veiros, L. F.; Kirchner, K.; Gonsalvi, L. Carbon dioxide hydrogenation catalysed by well-defined Mn(I)PNP pincer hydride complexes. *Chem. Sci.* **2017**, *8*, 5024−5029.
(39) Bielinski, E. A.; Förster, M.; Zhang, Y.; Bernskoetter, W. H.; Hazari, N.; Holthausen, M. C. Base-Free Methanol Dehydrogenation Using a Pincer-Supported Iron Compound and Lewis Acid Co-catalyst. *ACS Catal.* **2015**, *5*, 2404−2415.
(40) Heimann, J. E.; Bernskoetter, W. H.; Hazari, N. Understanding the Individual and Combined Effects of Solvent and Lewis Acid on CO_2 Insertion into a Metal Hydride. *J. Am. Chem. Soc.* **2019**, *141*, 10520−10529.
(41) Bielinski, E. A.; Lagaditis, P. O.; Zhang, Y.; Mercado, B. Q.; Würtele, C.; Bernskoetter, W. H.; Hazari, N.; Schneider, S. Lewis Acid-Assisted Formic Acid Dehydrogenation Using a Pincer-Supported Iron Catalyst. *J. Am. Chem. Soc.* **2014**, *136*, 10234−10237.
(42) Konno, H.; Kobayashi, A.; Sakamoto, K.; Fagalde, F.; Katz, N. E.; Saitoh, H.; Ishitani, O. Synthesis and properties of $[Ru(tpy)(4,4'\text{-}X_2bpy)H]^+$ (tpy = 2,2′:6′,2″-terpyridine, bpy = 2,2′-bipyridine, X = H and MeO), and their reactions with CO_2. *Inorg. Chim. Acta* **2000**, *299*, 155−163.
(43) Creutz, C.; Chou, M. H.; Hou, H.; Muckerman, J. T. Hydride Ion Transfer from Ruthenium(II) Complexes in Water: Kinetics and Mechanism. *Inorg. Chem.* **2010**, *49*, 9809−9822.
(44) Osipova, E. S.; Sedlova, D. V.; Gutsul, E. I.; Nelyubina, Y. V.; Dorovatovskii, P. V.; Epstein, L. M.; Filippov, O. A.; Shubina, E. S.; Belkova, N. V. Reactivity of Heterobimetallic Ion Pairs in Formic Acid Dehydrogenation. *Organometallics* **2023**, *42*, 2651.
(45) Decken, A.; Nikiforov, G. B.; Passmore, J. The reaction of TiF_4 with $Li(OC(CF_3)_2Ph)$: direct synthetic route to the lithium-titanium heterometallic fluoride bridged complex $\{Li(THF)_2TiF_3(OC(CF_3)_2Ph)_2\}_2$ and $Ti(OC(CF_3)_2Ph)_4$ alkoxide. *Dalton Trans.* **2006**, 4328−4334.
(46) Ohnishi, Y.-y.; Matsunaga, T.; Nakao, Y.; Sato, H.; Sakaki, S. Ruthenium(II)-Catalyzed Hydrogenation of Carbon Dioxide to Formic Acid. Theoretical Study of Real Catalyst, Ligand Effects, and Solvation Effects. *J. Am. Chem. Soc.* **2005**, *127*, 4021−4032.
(47) Wesselbaum, S.; Moha, V.; Meuresch, M.; Brosinski, S.; Thenert, K. M.; Kothe, J.; Stein, T. v.; Englert, U.; Hölscher, M.; Klankermayer, J.; et al. Hydrogenation of carbon dioxide to methanol using a homogeneous ruthenium-Triphos catalyst: from mechanistic investigations to multiphase catalysis. *Chem. Sci.* **2015**, *6*, 693−704.
(48) García-López, D.; Pavlovic, Lj.; Hopmann, K. H. To Bind or Not to Bind: Mechanistic Insights into $C-CO_2$ Bond Formation with Late Transition Metals. *Organometallics* **2020**, *39*, 1339−1347.
(49) Deziel, A. P.; Espinosa, M. R.; Pavlovic, Lj.; Charboneau, D. J.; Hazari, N.; Hopmann, K. H.; Mercado, B. Q. Ligand and solvent effects on CO_2 insertion into group 10 metal alkyl bonds. *Chem. Sci.* **2022**, *13*, 2391−2404.
(50) Ostapowicz, T. G.; Hölscher, M.; Leitner, W. CO_2 Insertion into Metal−Carbon Bonds: A Computational Study of RhI Pincer Complexes. *Chem.—Eur. J.* **2011**, *17*, 10329−10338.
(51) Schmeier, T. J.; Dobereiner, G. E.; Crabtree, R. H.; Hazari, N. Secondary Coordination Sphere Interactions Facilitate the Insertion Step in an Iridium(III) CO_2 Reduction Catalyst. *J. Am. Chem. Soc.* **2011**, *133*, 9274−9277.
(52) Filonenko, G. A.; Hensen, E. J. M.; Pidko, E. A. Mechanism of CO_2 hydrogenation to formates by homogeneous Ru-PNP pincer catalyst: from a theoretical description to performance optimization. *Catal. Sci. Technol.* **2014**, *4*, 3474−3485.
(53) Wei, Z.; Tian, X.; Bender, M.; Beller, M.; Jiao, H. Mechanisms of CoII and Acid Jointly Catalyzed Domino Conversion of CO_2, H_2, and CH_3OH to Dialkoxymethane: A DFT Study. *ACS Catal.* **2021**, *11*, 6908−6919.
(54) Johnee Britto, N.; Jaccob, M. DFT Probe into the Mechanism of Formic Acid Dehydrogenation Catalyzed by Cp*Co, Cp*Rh, and Cp*Ir Catalysts with 4,4′-Amino-/Alkylamino-Functionalized 2,2′-Bipyridine Ligands. *J. Phys. Chem. A* **2021**, *125*, 9478−9488.
(55) Yan, X.; Yang, X. Mechanistic Insights into Iridium Catalyzed Disproportionation of Formic Acid to CO_2 and Methanol: A DFT Study. *Organometallics* **2018**, *37*, 1519−1525.
(56) Ahlquist, M. S. G. Iridium catalyzed hydrogenation of CO_2 under basic conditions-Mechanistic insight from theory. *J. Mol. Catal. A Chem.* **2010**, *324*, 3−8.
(57) Tanaka, R.; Yamashita, M.; Chung, L. W.; Morokuma, K.; Nozaki, K. Mechanistic Studies on the Reversible Hydrogenation of Carbon Dioxide Catalyzed by an Ir-PNP Complex. *Organometallics* **2011**, *30*, 6742−6750.
(58) Zhang, M.; Liang, X.; Wang, Y.; Yang, H.; Liang, G. Insights into the Capture of CO_2 by Nickel Hydride Complexes. *Catalysts* **2022**, *12*, 790.
(59) Avasare, V. D. Ascendancy of Nitrogen Heterocycles in the Computationally Designed Mn(I)PNN Pincer Catalysts on the Hydrogenation of Carbon Dioxide to Methanol. *Inorg. Chem.* **2022**, *61*, 1851−1868.
(60) Liu, T.; Liu, Z.; Tang, L.; Li, J.; Yang, Z. Trans Influence of Boryl Ligands in CO_2 Hydrogenation on Ruthenium Complexes: Theoretical Prediction of Highly Active Catalysts for CO_2 Reduction. *Catalysts* **2021**, *11*, 1356.
(61) Zhang, Z.; Li, Y.; Hou, C.; Zhao, C.; Ke, Z. DFT study of CO_2 hydrogenation catalyzed by a cobalt-based system: an unexpected formate anion-assisted deprotonation mechanism. *Catal. Sci. Technol.* **2018**, *8*, 656−666.
(62) Pavlovic, Lj.; Vaitla, J.; Bayer, A.; Hopmann, K. H. Rhodium-Catalyzed Hydrocarboxylation: Mechanistic Analysis Reveals Unusual Transition State for Carbon−Carbon Bond Formation. *Organometallics* **2018**, *37*, 941−948.
(63) Pavlovic, Lj.; Pettersen, M.; Gevorgyan, A.; Vaitla, J.; Bayer, A.; Hopmann, K. H. Computational and Experimental Insights into Asymmetric Rh-Catalyzed Hydrocarboxylation with CO_2. *Eur. J. Org. Chem.* **2021**, *2021*, 663−670.
(64) Martínez-Martínez, A. J.; Tegner, B. E.; McKay, A. I.; Bukvic, A. J.; Rees, N. H.; Tizzard, G. J.; Coles, S. J.; Warren, M. R.; Macgregor, S. A.; Weller, A. S. Modulation of σ-Alkane Interactions in $[Rh(L_2)(alkane)]^+$ Solid-State Molecular Organometallic (SMOM) Systems by Variation of the Chelating Phosphine and Alkane: Access to η^2,η^2-σ-Alkane Rh(I), η^1-σ-Alkane Rh(III) Complexes, and Alkane Encapsulation. *J. Am. Chem. Soc.* **2018**, *140*, 14958−14970.
(65) The naming of the η1-σ-intermediate is based on the nomenclature used in ref 64.

https://doi.org/10.1021/acs.organomet.3c00342
Organometallics 2023, 42, 3025−3035

(66) Luo, C.; Li, L.; Yue, X.; Li, P.; Zhang, L.; Yang, Z.; Pu, M.; Cao, Z.; Lei, M. pH-Dependent transfer hydrogenation or dihydrogen release catalyzed by a $[(\eta^6\text{-arene})RuCl(\kappa^2\text{-N,N-dmobpy})]^+$ complex: a DFT mechanistic understanding. *RSC Adv.* **2020**, *10*, 10411−10419.
(67) Bernskoetter, W. H.; Hazari, N. A Computational Investigation of the Insertion of Carbon Dioxide into Four- and Five-Coordinate Iridium Hydrides. *Eur. J. Inorg. Chem.* **2013**, *2013*, 4032−4041.
(68) Sen, A.; Ansari, M.; Rajaraman, G. Mechanism of Hydroboration of CO_2 Using an Fe Catalyst: What Controls the Reactivity and Product Selectivity? *Inorg. Chem.* **2023**, *62*, 3727−3737.
(69) Jiang, Y.; Blacque, O.; Fox, T.; Berke, H. Catalytic CO_2 Activation Assisted by Rhenium Hydride/$B(C_6F_5)_3$ Frustrated Lewis Pairs-Metal Hydrides Functioning as FLP Bases. *J. Am. Chem. Soc.* **2013**, *135*, 7751−7760.
(70) Buil, M. L.; Cabeza, J. A.; Esteruelas, M. A.; Izquierdo, S.; Laglera-Gándara, C. J.; Nicasio, A. I.; Oñate, E. Alternative Conceptual Approach to the Design of Bifunctional Catalysts: An Osmium Germylene System for the Dehydrogenation of Formic Acid. *Inorg. Chem.* **2021**, *60*, 16860−16870.
(71) Frisch, M. J.; Trucks, G. W.; Schlegel, H. B.; Scuseria, G. E.; Robb, M. A.; Cheeseman, J. R.; Scalmani, G.; Barone, V.; Petersson, G. A.; Nakatsuji, H.; Li, X.; Caricato, M.; Marenich, A. V.; Bloino, J.; Janesko, B. G.; Gomperts, R.; Mennucci, B.; Hratchian, H. P.; Ortiz, J. V.; Izmaylov, A. F.; Sonnenberg, J. L.; Williams; Ding, F.; Lipparini, F.; Egidi, F.; Goings, J.; Peng, B.; Petrone, A.; Henderson, T.; Ranasinghe, D.; Zakrzewski, V. G.; Gao, J.; Rega, N.; Zheng, G.; Liang, W.; Hada, M.; Ehara, M.; Toyota, K.; Fukuda, R.; Hasegawa, J.; Ishida, M.; Nakajima, T.; Honda, Y.; Kitao, O.; Nakai, H.; Vreven, T.; Throssell, K.; Montgomery, J. A., Jr.; Peralta, J. E.; Ogliaro, F.; Bearpark, M. J.; Heyd, J. J.; Brothers, E. N.; Kudin, K. N.; Staroverov, V. N.; Keith, T. A.; Kobayashi, R.; Normand, J.; Raghavachari, K.; Rendell, A. P.; Burant, J. C.; Iyengar, S. S.; Tomasi, J.; Cossi, M.; Millam, J. M.; Klene, M.; Adamo, C.; Cammi, R.; Ochterski, J. W.; Martin, R. L.; Morokuma, K.; Farkas, O.; Foresman, J. B.; Fox, D. *Gaussian 16 Rev. C.01*; Gaussian Inc.: Wallingford, CT, 2016.
(72) Perdew, J. P.; Ernzerhof, M.; Burke, K. Rationale for mixing exact exchange with density functional approximations. *J. Chem. Phys.* **1996**, *105*, 9982−9985.
(73) Adamo, C.; Barone, V. Toward reliable density functional methods without adjustable parameters: The PBE0 model. *J. Chem. Phys.* **1999**, *110*, 6158−6170.
(74) Grimme, S.; Ehrlich, S.; Goerigk, L. Effect of the damping function in dispersion corrected density functional theory. *J. Comput. Chem.* **2011**, *32*, 1456−1465.
(75) Tomasi, J.; Mennucci, B.; Cammi, R. Quantum Mechanical Continuum Solvation Models. *Chem. Rev.* **2005**, *105*, 2999−3094.
(76) Cossi, M.; Rega, N.; Scalmani, G.; Barone, V. Energies, structures, and electronic properties of molecules in solution with the C-PCM solvation model. *J. Comput. Chem.* **2003**, *24*, 669−681.
(77) Becke, A. D. Density-functional exchange-energy approximation with correct asymptotic behavior. *Phys. Rev. A* **1988**, *38*, 3098−3100.
(78) Weigend, F.; Ahlrichs, R. Balanced basis sets of split valence, triple zeta valence and quadruple zeta valence quality for H to Rn: Design and assessment of accuracy. *Phys. Chem. Chem. Phys.* **2005**, *7*, 3297−3305.
(79) Hay, P. J.; Wadt, W. R. Ab initio effective core potentials for molecular calculations. Potentials for K to Au including the outermost core orbitals. *J. Chem. Phys.* **1985**, *82*, 299−310.
(80) Hopmann, K. H. How Accurate is DFT for Iridium-Mediated Chemistry? *Organometallics* **2016**, *35*, 3795−3807.
(81) Sparta, M.; Riplinger, C.; Neese, F. Mechanism of Olefin Asymmetric Hydrogenation Catalyzed by Iridium Phosphino-Oxazoline: A Pair Natural Orbital Coupled Cluster Study. *J. Chem. Theory Comput.* **2014**, *10*, 1099−1108.
(82) Younesi, R.; Veith, G. M.; Johansson, P.; Edström, K.; Vegge, T. Lithium salts for advanced lithium batteries: Li−metal, Li−O_2, and Li−S. *Energy Environ. Sci.* **2015**, *8*, 1905−1922.
(83) Xu, K. Nonaqueous Liquid Electrolytes for Lithium-Based Rechargeable Batteries. *Chem. Rev.* **2004**, *104*, 4303−4418.
(84) Knorr, R.; Lattke, E.; Ruhdorfer, J.; Ferchland, K.; von Roman, U. Why is cis/trans stereoinversion with $Li^+(THF)_4$ migration across the phenyl ring of α-lithiostyrene accelerated by two ortho-methyl groups? *Tetrahedron* **2018**, *74*, 1621−1631.
(85) Yun, S.-H.; Han, S.-D.; Borodin, O.; Seo, D. M.; Afroz, T.; Sommer, R. D.; Henderson, W. A. Solvate Structures and Computational/Spectroscopic Characterization of $LiCF_3SO_3$ Electrolytes. *J. Phys. Chem. C* **2022**, *126*, 18251−18265.
(86) Luo, M.; Li, J.; Xiao, Q.; Yang, S.; Su, F.; Ma, M. Efficient and selective carbonyl hydroboration catalyzed by a lithium NCN-Pincer magnesiate complex $[Li(THF)_4][NCN\text{-}MgBr_2]$. *J. Organomet. Chem.* **2018**, *868*, 31−35.
(87) Huang, W.; Frech, R.; Wheeler, R. A. Molecular structures and normal vibrations of trifluoromethane sulfonate ($CF_3SO_3^-$) and its lithium ion pairs and aggregates. *J. Phys. Chem.* **1994**, *98*, 100−110.
(88) Only compared rates between LAs (molecularity is differernt in absence of LA and cannot be compared directly).
(89) Although we cannot exclude that a cyclic TS1 may exist.
(90) Barakat, M. Mechanistic DFT Studies on Carbon Dioxide and Carbonyl Compounds Insertion into Transition Metal-Hydride Complexes 2022, (Doctoral thesis), American University Of Beirut. http://hdl.handle.net/10938/23283.
(91) Liu, X.; Qiu, B.; Yang, X. Bioinspired Design and Computational Prediction of SCS Nickel Pincer Complexes for Hydrogenation of Carbon Dioxide. *Catalysts* **2020**, *10*, 319.
(92) Moni, S.; Mondal, B. Correlation between Key Steps and Hydricity in CO_2 Hydrogenation Catalysed by Non-Noble Metal PNP-Pincer Complexes. *Catalysts* **2023**, *13*, 592.

https://doi.org/10.1021/acs.organomet.3c00342
Organometallics 2023, 42, 3025−3035